ijrr

The International Journal of Robotics Research
29(12) 1550–1564
© The Author(s) 2010
Reprints and permission:
sagepub.co.uk/journalsPermissions.nav
DOI: 10.1177/0278364910370217
ijr.sagepub.com
SAGE

Design and field experimentation of a prototype Lunar prospector

David Wettergreen, Scott Moreland, Krzysztof Skonieczny, Dominic Jonak, David Kohanbash and James Teza

Abstract

Scarab is a prototype rover for Lunar missions to survey resources in polar craters. It is designed as a prospector that would use a deep coring drill and apply soil analysis instruments to measure the abundance of elements of hydrogen and oxygen and other volatiles including water. Scarab's chassis can adjust the wheelbase and height to stabilize its drill in contact with the ground and can also adjust posture to better ascend and descend steep slopes. This enables unique control of posture when moving and introduces new planning issues. Scarab has undergone field testing at Lunar-analog sites in Washington and Hawaii in an effort to quantify and validate its mobility and navigation capabilities. We report on results of the experiments in slope ascent and descent and in autonomous kilometer-distance navigation in darkness.

Keywords

Space and planetary robotics, rough-terrain mobility, autonomous navigation, Hawaii field experiment

1. Introduction

The possibility of water on the Moon gained evidence with the Clementine spacecraft in 1994 and was confirmed 3 years later by neutron detectors on the Lunar Prospector, which showed elevated levels of hydrogen in Lunar polar craters (Spudis, 2006). Observations from the Chandrayaan-1 spacecraft of larger than expected quantity and distribution of hydrogen, either as hydroxyl (OH) or water (H_2O), in craters around the moon (Clark, 2009; Pieters et al., 2009) is impetus for understanding and utilizing this resource to create fuel, air, and water for lunar exploration.

To discover and measure the resources of the moon, robotic vehicles will have to survive extremes from blazing sunlight to frigid darkness as well as dust, vacuum, and isolation. Scarab is a prospecting rover developed to perform the necessary science operations to locate volatiles and validate *in situ* resource utilization methods (Sanders et al., 2009) (Figure 1). It is a concept vehicle for terrestrial testing and does not address aspects of a Lunar mission associated with thermal extremes and power generation. Scarab is configured to deploy a deep coring drill (Boucher, 2008) and to transport soil analysis instruments (Muscatello et al., 2008) that have also been designed to work on Earth but allow for future Lunar implementation. The vehicle design employs a passive kinematic suspension with active posture adjustability. Expanding the side-frames increases the front–rear wheel separation and decreases the body height above the ground. The chassis can lower to contact the ground to stabilize the coring drill and can also adjust to control roll, meaning rotation about its longitudinal axis, by independently adjusting its side frames. This allows it to drive cross-slope and turn switchbacks to better ascend and descend unconsolidated soil.

Scarab is designed for operation on and within Lunar craters, particularly in polar regions. Because the interior slopes and crater floor are sometimes in shadow, or in some cases in permanent darkness, active sensing methods are needed for terrain modeling and autonomous navigation. Scarab employs laser range scanners with autonomous navigation algorithms to build models of the surrounding terrain to detect obstacles and then determine efficient and safe paths.

In this article we review results from field experiments at Moses Lake Dunes, WA, and Mauna Kea, HI, to measure and verify the prototype rover's ability to meet the demands of a Lunar-crater prospecting mission.

2. Rover Configuration

Scarab was conceived as a work machine with a serialized mission: drive, charge batteries, drill, charge again, analyze soil samples, charge and repeat. The number of repetitions might be 25, leading to 25 kilometers of traverse, 25 cores,

The Robotics Institute, Carnegie Mellon University, Pittsburgh, PA

Corresponding author:
David Wettergreen The Robotics Institute, Carnegie Mellon University, Pittsburgh, PA 15212, USA
Email: dsw@ri.cmu.edu

Fig. 1. Scarab Lunar rover prototype is designed to transport a coring drill and instrument payload while operating in the permanent darkness of polar craters. Shown in Moses Lake Dunes, WA.

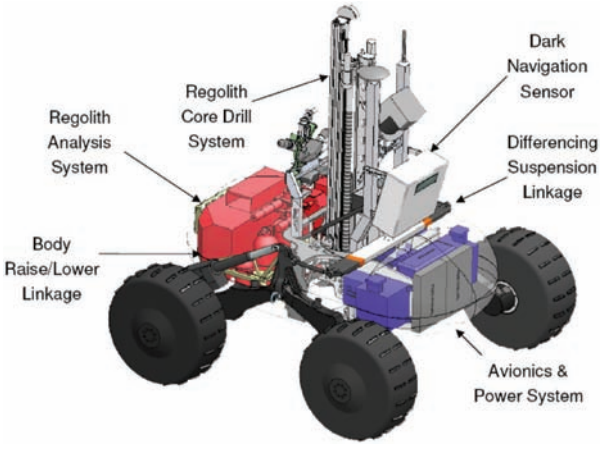

Fig. 2. Scarab rover configuration showing placement of sensors, avionics and payload. There are drive motors in each of four wheels and two linkages for adjusting the side-frame height. An averaging linkage allows all four wheels to maintain ground contact in rough terrain.

and 25 sites surveyed. For some craters such as Shackleton at the South Pole of the Moon, 100 repetitions might be more desirable to characterize the environment and resources. We estimate this would require approximately 9 months to complete on the limited power delivered by a small (120-W) isotope generator.

There are many factors effecting the rover configuration but the drill mechanism and its operation dominate. The requirement to transport and stabilize a deep coring drill is literally central to the design while requirements for ascent and descent in cratered terrain shaped many aspects and fine details.

Drilling requires a platform into which thrust loads, torques and vibrations are transmitted and hole alignment is maintained. Placement of the drill in line with the vehicle's center-of-mass maximizes the mass that can be applied in downward force (Figure 2). Drilling operations receive three benefits from this feature: first, lowering the chassis allows the full stroke of the drill to be used in the soil resulting in mass savings overall; second, the rover can lean and therefore re-stabilize and place the rover's center-of-mass over the drill core; lastly, under low-gravity conditions, the drill torque can be counteracted further by spreading the rover wheelbase to increase the leverage arm from the wheels to the drill.

As with all space systems, reducing mass is vital due to the cost of transport to the moon, but in this case there is a counteracting requirement. The drill payload is significant (50 kg) and imposes forces on the chassis during transport and while interacting with the ground. This poses a unique requirement on the rover system in that a minimum mass must be met in order to provide enough static load to react to drilling thrust and torque. The rationale for the vehicle weight and size is based on the 1 m long, 3 cm diameter drill that is likely to be employed in a lunar mission. Drill thrusts are expected to reach 250 N and 50 Nm torque. The system weight on lunar surface must react drilling 250 N down-force and maintain 150 N on wheels for stability against uplift and spin, therefore total weight on the Lunar surface must be greater than 400 N. The weight in Lunar gravity (400 N/1.622 m s^{-2} = 250 kg) leads to a minimum 250 kg vehicle mass (Bartlett et al., 2008).

We undertook a study of configurations (described by Bartlett (2008)) and an early insight was that due to power limitations the rover speed would be low and thus forces imposed on it during locomotion would also be slowly evolving. A dynamic suspension, for example using springs, torsion tubes, dampers, would not be needed to absorb impacts and could be unstable when carrying high loads or reacting to drilling forces and torques. A dynamic suspension using high-speed actuators to comply with terrain was also not justifiable. Thus, kinematic suspensions, the class of suspensions that employ balanced, passive linkages that are unsprung and undamped so that the wheels can conform freely to the terrain, became the preferred chassis type for the requirements of this lunar rover (Bartlett, 2008).

Kinematic suspensions are common for slow-moving vehicles operating in rough terrain, a prime example among planetary rovers are the six-wheel rocker-bogie designs of the Mars Exploration Rovers, Sprit and Opportunity (Lindemann and Voorhees, 2005), as well as their predecessor Sojourner and their successor the Mars Science Laboratory. In fact, most planetary rovers including the Soviet Lunokhods and the future European ExoMars rover employ kinematic suspensions. The American Lunar Roving Vehicle is a notable exception, as it was intended for relatively high speeds and astronaut drivers. There are prior examples of planetary rover concepts that can change their kinematic suspension dating back to early Soviet Lunar concepts. Terrestrial prototypes include the Jet Propulsion Laboratory NanoRover (Wilcox and Jones, 2000) and Sample Return Rover (SRR) (Tarokh and McDermott, 2007).

Iagnemma et al. (2000) identify the benefit of articulating the kinematic suspension of the SRR to improving rough terrain tip-over stability. The SRR has independent

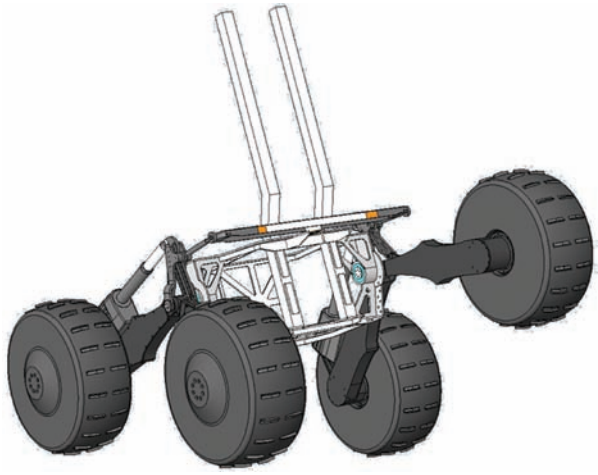

Fig. 3. Scarab rover passive pitch averaging between left and right side-frames. Pivots (mechanical releases) between the two side frames and body allow them to freely rotate with respect to each other. A differencing linkage constrains the body to the average pitch between the side frames.

Fig. 4. Change to each side-frame angle, by adjustment of a linear actuator, changes the wheel base and ride height.

control of side-frame wheel separation, although unlike Scarab this was not primarily driven by the need to lower the robot into ground contact and as a result the height adjustment is only a fraction of the ground clearance (Tarokh and McDermott, 2007). Iagnemma and Dubowsky (2004) review the complexity of wheel/terrain interaction for passively compliant suspensions in deformable materials and develop the necessary models. We have recently worked to model and apply suspension adjustment in configuration space path planning (Furlong et al., 2009).

For Scarab a four-wheel skid steer (differential) drive configuration was chosen for the mobility platform for its stiffness and relative simplicity (compared with explicit steering). The high-stiffness suspension and chassis design is important for both skidding and drilling.

The chassis conforms to the terrain as the rover drives. The suspension has passive and active elements for improved traction on rough and sloped terrain. The passive element, sometimes called an averaging (or differencing) linkage provides a mechanical release allowing the two suspension side frames to pivot independently and effectively three contact points with the ground. As the center-of-mass of the rover is located midway between the side frames, equal loading occurs on all four wheels on uneven terrain. This differencing linkage is similar in concept to the mechanism in the Nomad rover although the design is different to maintain open payload volume at the center of the chassis (Rollins et al., 1998).

The active element of the suspension, the two adjustable side frames, enables the rover to lower the chassis into contact with the ground and allows it to level its body, leading to increased stability and traction efficiency. Each side-frame consists each of two rocker arms, two wheels, in-hub actuators in each wheel and a linear actuator for rocker-arm sweep angle adjustment. Each side frame can freely rotate (in pitch) with respect to the other, while the rover chassis, pitches half the angle in between the two. The independent pivot of the side-frames allows for the suspension to conform to uneven and rough terrain (Figure 3) while reducing the amplitude of body pitch where sensors are located.

Scarab actively controls its roll using the rocker arms by changing the height of each side independently. The angle between each rocker arm is adjusted by a linear actuator, allowing for a change in height/wheelbase of each side-frame (Figure 4). This provides active control of the rover body roll-axis, leading to the ability to control the placement of center of gravity about this axis, leveling the rover body.

Scarab uses relatively large wheels (71 cm diameter) for a planetary rover. They provide increased performance on loose terrain and rocks, and coupled with the high torque (915 Nm) in-hub actuator and the averaging suspension, they enable the rover to easily roll over rocks of wheel radius (35.5 cm). We have observed during field trials that an increased normal loading is produced in the wheels encountering an obstacle as the thrust of wheels on the ground increases traction on hard surfaces and allows Scarab to overcome obstacles up to the wheel diameter. In addition to size, compliant wheels that generate low ground pressure (<10 psi) and can be manufactured from Lunar-relevant material to aid in surmounting loose terrain and slopes.

The Scarab rover physical specifications are summarized in Table 1. The static pitch-over and roll-over angles were experimentally verified on an instrumented tilt bed (Bartlett et al., 2008).

Table 1. Scarab Rover Specifications

Mass	280 kg
Weight	2740 N Earth surface
	450 N Lunar surface
Locomotion speed	3–6 cm s–1
Wheel diameter	71 cm
Track width	1.4 m
Wheel actuator torque	915 Nm maximum
	(85% rover weight in rim-pull)
Wheelbase	0.8–1.4 m
	1.2 m nominal
Aspect ratio	1:1.0 low stance
(track/wheelbase)	1:1.2 nominal stance
	1:1.7 high stance
CG planar location	On geometric center
CG height	0.48 m low stance
	0.64 m nominal stance
	0.74 m high stance
Static pitch-over	56° low stance
	43° nominal stance
	30° high stance
Static roll-over	61° low stance
	53° nominal stance
	49° high stance
Maximum straddle	0.55 m
Minimum straddle	0.00 m (ground contact)

3. Field Sites

Testing Scarab in the field has been critical in proving the concept for Lunar mobility and quantifying performance. Field experimentation was conducted in Moses Lake Sand Dunes, WA, in June 2008 and on Mauna Kea, HI, in November 2008. Characterization of the Scarab rover mobility system has also been undertaken at the NASA Glenn Research Center. Experiments have been conducted under various conditions with several findings of importance although it is understood that continued experimentation is needed to provide a fully validated performance model and, most importantly, to enable extrapolation of terrestrial results to the Lunar environment.

Moses Lake Sand Dunes in Eastern Washington State (47.07°N, 119.28°W) was chosen as a test site by the NASA Human Robotic Systems program for its varied terrain (slopes, pits, etc.), low moisture content, varied soil types (strengths, size distribution) and wide open spaces. These qualities provided grounds for mobility traction testing and long-distance dark navigation traverses. The large open areas, varying from flat ground to steep inclines, also provided terrain for robotic sub-surface mapping and site surveying (Fong et al., 2008), combined crew mobility vehicle and extra-vehicular activities (Harrison et al., 2008) and robotic cargo handling and transportation (Wilcox et al., 2007). Position estimation and obstacle detection, steep slope ascent/descent in loose soil and tests of new slope climbing techniques and algorithms were the focus of these field tests.

The Lunar-analog site located on Mauna Kea in Hawaii (19.76°N, 155.46°W) is at high altitude with dry, deep, basaltic volcanic ash that allows repeated mobility and navigation experiments. (Fox et al., 2009), Figure 6 The soil composition and mechanical properties at this site are ideal for regolith drilling and sampling experiments. The objectives of these tests, organized by the NASA In Situ Resource Utilization program were to demonstrate roving, drilling, sample acquisition, processing and analysis: the complete sequence of Lunar prospecting activities. The rover was to autonomously traverse kilometers of rough terrain, inspect a drill site, drill to 1 m depth, process the core sample to analyze the composition of the captured soil and demonstrate extraction of water from soil. This would be the first demonstration of a complete Lunar prospecting scenario.

Fig. 5. Examples of climbing and suspension capability: surmounting a stable, wheel-diameter rock (upper left), active body-roll aiding in slope ascent (upper right), climbing offset obstacles (lower left), and egress from a rover-scale crater (lower right).

4. Mobility Experiments

The approach to mobility testing with Scarab has been to characterize performance, through repeated experiments, and then understand performance in a wide range of conditions. The kinematic design of the rover, although similar in its side-frame adjustment to the JPL Sample Return Rover (Iagnemma et al., 2000), has not been examined in the relevant variety of terrain materials and slopes to understand its efficacy on the Moon. For this reason, it is important to validate models of the mobility system and the rover's ability to safely carry a scientific payload. In addition, performance metrics for traction and energetics are determined to evaluate chassis and wheel designs.

Three specific experiments were performed in laboratory and field sites: drawbar pull, cross-slope, and slope ascent. The metrics applied during these experiments focused not only on the rover as a whole, but also investigated individual aspects of the mobility system, such as wheel design and driving methods, so the effects of specific design parameters could be realized.

The Scarab mobility experiments focused on traction and slope ascent but not step obstacle performance.

Fig. 6. Scarab rover with drill and instrument payload and Lunar wheels in fine basaltic soil at 3,000 m elevation on Mauna Kea in Hawaii.

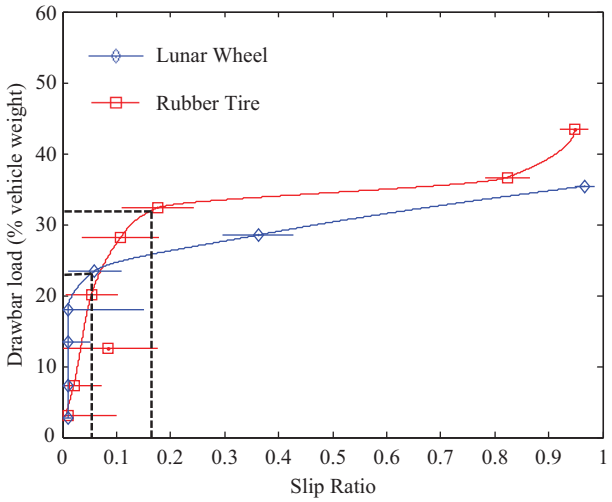

Fig. 7. Drawbar load versus slip curve. Inflection where slip becomes significant is noted for two types of wheels (slightly over 20% of vehicle weight for lunar wheels (shown in Figure 6), and over 30% for rubber tires (shown in Figure 1)). By convention, the slip ratio is shown on the horizontal axis despite being the dependent variable (Bekker, 1956). Thus, error bars are also in the horizontal direction. The error bars are calculated from the standard error of the rover velocity, and thus slip, observed at any given loading. Note: dotted lines between data points are for visual aid only, and do not represent trend modeling.

Rock/step obstacles in the field vary widely in shape, size, and material (confounding systematic analysis), so field observation provides the best sense of vehicle performance in an analog setting for these obstacle types. As noted, rocks of wheel radius and even diameter are regularly surmounted (Figure 5). In addition, rocks that would be considered insurmountable are primarily avoided by the vehicle's navigation system.

4.1. Drawbar Pull

A widely used metric for measuring the total tractive ability of a vehicle is *drawbar pull* which is the load a vehicle can pull while maintaining progress (Wong, 2001). In terms of wheel–soil interaction, the drawbar pull value is the thrust produced by the wheels minus the sum of all resistances acting on the wheels. On a load–slip curve, the maximum drawbar pull value corresponds to an inflection, or "knee", where the soil fails and the wheel quickly enters the high-slip regime (indicated in Figure 7). In order to create this curve, a range of loads must be applied in steps that span 0% to 100% slip at steady-state response. The drawbar pull value is quite informative when comparing different aspects of wheel and suspension designs during physical testing but can also be used for estimating the slope a vehicle can continuously ascend under low slip for a specified material. Drawbar pull is usually expressed as pull load normalized by vehicle weight (Bekker, 1956).

Our experimental setup for conducting drawbar pull measurements in the field is shown in Figure 8. A load cell measures the resistance of the towed mass, which is incrementally increased during the test by the addition of sandbags. In laboratory tests, a cable mechanism with variable tension control takes the place of a towed mass. Wheel slip is determined by comparing wheel rotation speeds to rover velocity calculated at 1 Hz from external position measurements by a surveying total station. The total station is a Leica TCRA 1103 robotic model with automatic track feature for moving targets and custom communication software for real-time synchronization of its measurements to rover telemetry. The position data is transmitted wirelessly via laptop to the Scarab rover onboard computer for simultaneous logging of telemetry including wheel current and angular position, rover position, and drawbar pull load.

The drawbar pull tests also permit evaluation of the effects that rover mass properties, wheel design, and soil properties have on tractive performance. Both drawbar pull (load–slip curve) and the self-propelled power values measured from the tests were used as metrics to quantify performance.

As an example of the merit of drawbar pull evaluation, Figure 9 illustrates the effect that normal load (per wheel) has on overall traction. It is evident from the load–slip curves that the normalized drawbar pull values decrease with higher normal loads and higher ground pressures.

Wheel design is another factor that be evaluated with this technique: comparing different wheels with other parameters kept constant. It should be noted that some wheel types and suspensions create a slip response that does not produce a clear "knee" in the load–slip curve. As soil types relevant to planetary robotics seem to fail at between 10–30% wheel slip, evaluation of maximum drawbar pull is chosen at 20% slip in cases with no inflection.

Of specific interest during the field experiments was quantifying the performance of various wheel designs. Traction and driving efficiency were measured during drawbar pull experiments and compared with a rubber tire as a common baseline (although rubber is not a viable material in the

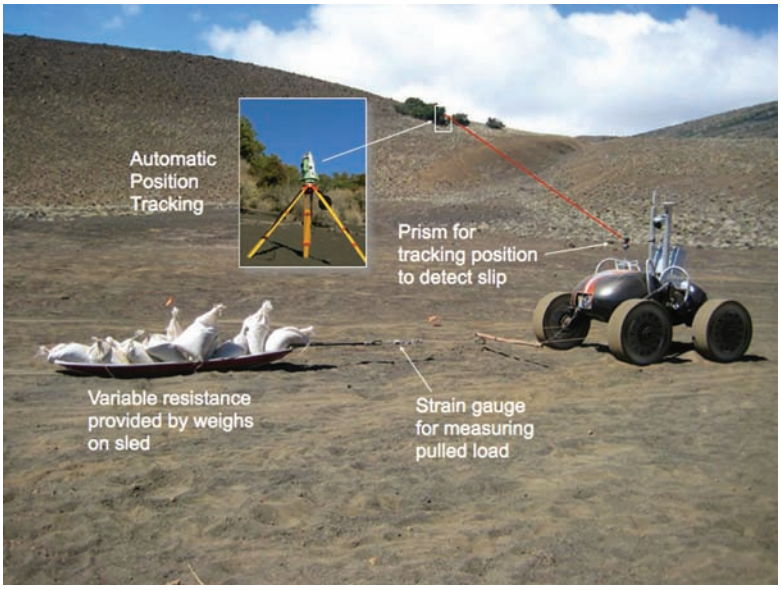

Fig. 8. Drawbar pull experimental setup: weight is added to the sled with the rover in motion while slip is continuously monitored. The rover is commanded at a constant 4.5 cm s^{-1} velocity (although slip reduces speed) and true position is tracked.

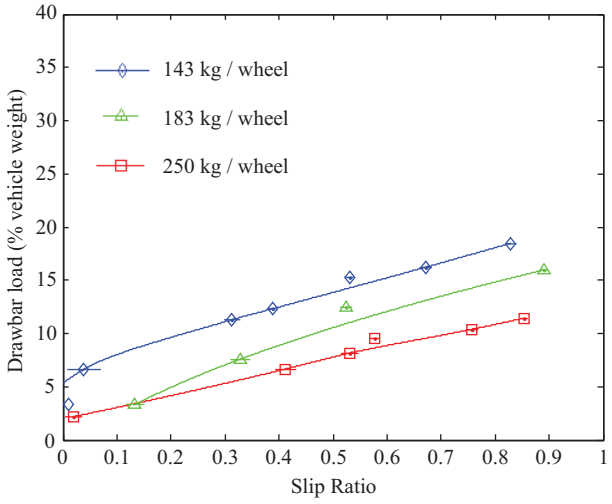

Fig. 9. Increasing wheel load (mass per wheel) decreases normalized drawbar pull.

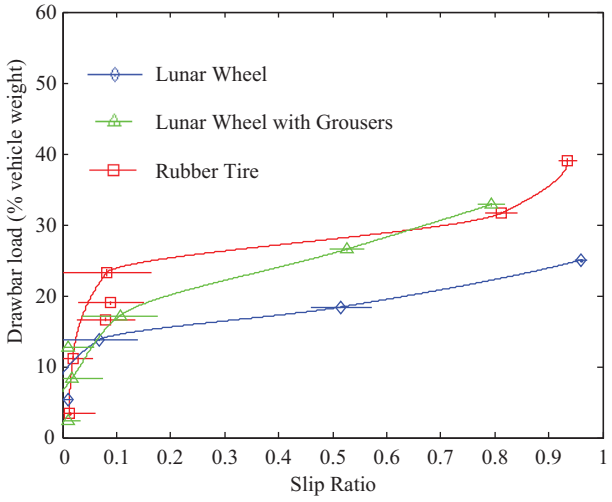

Fig. 10. Comparison of three wheel types with other conditions (wheel load, soil type) held constant. Addition of grousers improved traction, especially at higher loads.

extremes of temperature and vacuum on the moon). The self-propelled power (locomotion power, flat ground with sinkage) is a key indicator of wheel motion efficiencies and resistances. Compliant wheels with larger diameter and width have larger contact area, lower ground pressure, reduced sinkage and ultimately lower motion resistances. In soft soils, such as volcanic ash, the lunar relevant wheel design was shown to have a wheel motion resistance of $\sim 5\%$ vehicle weight, while the rubber tires were $\sim 22\%$ (total all four wheels). This resulted in a 50% savings in locomotion power above the baseline wheel. This is consistent with observation of wheels with aggressive tread patterns, such as grousers, which lead to high soil disturbance and therefore greater motion resistances.

The drawbar pull load at soil failure was also measured by using the normalized load value at the first knee in the curve. This metric for tractive performance is able to evaluate the effects of changes to wheel design or to directly compare multiple wheels types. As an example, an increase in traction (drawbar pull) was desired of the Lunar wheel. The addition of grousers (originally rough surface only) to this wheel was tested to examine the effect on traction and power efficiency. The increase in drawbar pull at low slip (<20%) was minimal, although there was a large increase in thrust during high slip. Operating at a high slip condition is undesirable as it may not be continuous due to large quantities of material transport underneath the wheel.

Table 2. Drawbar Pull and Self-propelled Power

Variable	Site	Drawbar pull (% rover weight)	Nominal drive power
GRC-1 loose	GRC slope	27%	120 W
GRC-1 compacted	GRC slope	30%	103 W
Best 530 loose	GRC slope	30%	105 W
Basaltic volcanic	Mauna Kea	28%	158 W
Loose sand	Moses Lake	20%	134 W
Heavy payload (25% increase)	GRC slope	31%	120 W
Shallow top layer, 1" depth	Mauna Kea	39%	103 W
Lunar wheel design	Mauna Kea	23%	100 W

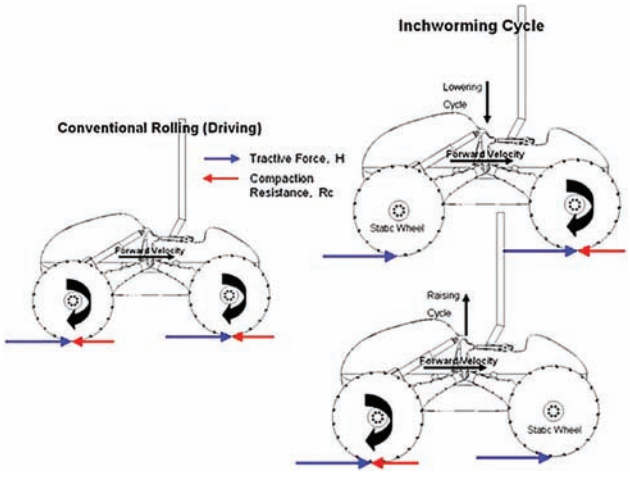

Fig. 11. Conventional rolling versus inch-worming where one wheel pair is synchronized to the side-arm expansion/contraction and the other reacts forces into the ground. In the lowering phase the rear wheel is static and the front wheel drives forward, and in the raising phase the front wheel is fixed with respect to the ground and the rear wheel drives forward.

In addition, a high degree of slip-induced sinkage is produced leading to high power draw and high risk of getting stuck in wheel ruts. The grousers implemented were thin and relatively sparse (two always in contact with ground patch), as such, there was little increase in the self-propelled power draw due to the low soil disturbance.

An important observation from the drawbar pull tests are the range of tractive values that occur with changing vehicle and terrain parameters. Table 2 shows varying soil, rover and wheel parameters and their resulting effects on net traction (drawbar pull) and self-propelled power. For high-bearing-strength materials such as Lunar regolith, the degree of looseness and compaction results in varied traction and power. The overall mass (given even loading of wheels) does effect the normalized drawbar pull value (Figure 9 and Table 2) proportionally to the mass increase up to a limit. It should be noted for extremely low bearing strength materials, this does not hold true as a result of excessive sinkage.

Table 2 compiles drawbar pull and nominal drive power in a variety of soil types: commercial sand mixes, including Best 530 and GRC-1 (Oravec et al., 2009), and natural soils at Moses Lake and Mauna Kea.

Experiments involving different traction surfaces, wheel diameter and ground pressures have shown a large range of drawbar pull values. Differences of 50% have been achieved through traction surface/grouser modifications. Lowering ground pressure and reducing sinkage can have a large effect on traction and results have shown to have large differences in driving power, showing up to 50% during experiments. Drawbar pull tests performed as laboratory and field experiments have highlighted wheel design as a leading element in tractive and power performance. This is an important realization as wheel design is generally independent of the mobility system suspension design and can be optimized for traction and power efficiencies.

Additional control methods can also lead to increased tractive performance in varied terrain types. Techniques such as "inch-worming" and actively controlled center-of-mass positioning can greatly increase the mobility of a rover whether on flat ground or sloped terrain.

4.2. Inch-worming

The motion of a vehicle relative to non-rolling wheels, by change of chassis length, is referred to as push-rolling (Bekker, 1956), but when the body raises and lowers while expanding and contracting, like an inch-worm, we refer to it as inch-worming. Scarab can exhibit this interesting driving mode (Figure 11).

To begin the cycle of inch-worming, the body lowers while expanding the side-frames hence the wheelbase and rolling the front wheels forward while the rear wheels remain fixed relative to the ground. Once the limit of body expansion is reached, the body raises and the wheel base contracts while the rear wheels roll forward and the front wheels remain fixed. To implement this motion on Scarab, the fixed wheels must actually counter-rotate in synchrony with the expanding or contracting side frame; if they were to be locked they would rotate in the soil as the side frame moves and thereby break their static contact with the soil. It has taken considerable effort to model and calibrate the wheel velocity to the side-frame actuation to achieve this synchronization.

Keeping two of Scarab's four wheels static relative to the ground eliminates the compaction resistances of these two wheels. In addition, a braked (static) wheel has been shown to produce larger thrust beyond that of a rolling

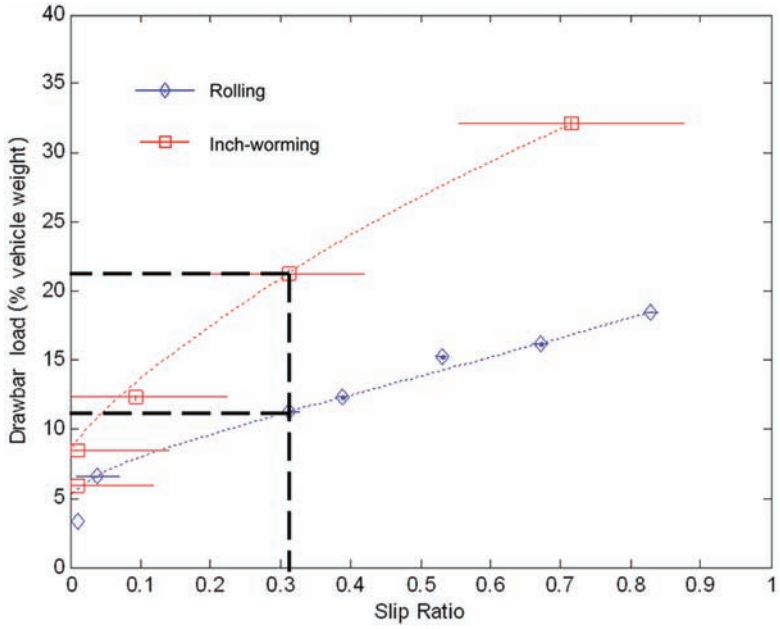

Fig. 12. Load–slip curve comparing rolling and inch-worming with other parameters (mass, wheels, soil type and condition) held constant shows doubling of drawbar pull.

wheel (Von Sybel and Gross-Scharmann, 1961). Higher thrust and lower resistance results in substantial traction improvements.

Experimentally we have found that the inch-worming technique even succeeds when wheels become entrenched under high slip. This allows the rover to move forward (or retreat) from entrapment. Techniques such as inch-worming are thus highly valuable, allowing the vehicle to overcome such difficult situations.

Initial laboratory testing of inch-worming has shown substantial increases in the net traction produced by this mode of locomotion. Figure 12 shows an approximate doubling in drawbar pull over conventional rolling (at 30% slip) in Lunar simulant soil. The inch-worming gains result from both increased thrust and lowered resistances. It was therefore important to have both these aspects present during testing. The drawbar pull experiments were conducted in GRC-1 with rigid wheels and a sandpaper-like traction surface. As a result, a typical wheel sinkage ($\sim$1 or 2 cm) and low shear strength situation was achieved for experimentation. This would be similar to the obstacle a slope would create in terms of the traction situation.

Limited testing of inch-worming has been conducted in the field. In particular, the performance on slopes has not shown the maximum angle ascendable. Inferring the gain in slope inch-worming provides from Figure 12, shows about a 6° increase provided by the inch-worming maneuver. It should be noted that these results are from the use of rigid wheels (which have relatively low drawbar pull values) and the expected absolute gain would be much higher for wheels with higher performance. These gains are (but not always) in addition to other changes that can be made to a mobility system to increase tractive performance. For example, an extremely low ground pressure wheel was tested on Scarab which produced a high drawbar pull (and high maximum slope). Although the low ground pressure wheels have less motion resistances (due to low sinkage), inch-worming would additionally increase the vehicle drawbar pull by increasing individual wheel thrusts. In this case inch-worming would be increasing the pure tractive efficiency of the wheels but have little effect on reducing resistances. Therefore, the increase in drawbar pull would be less than double but still significant.

Fig. 13. Conventional posture normal to the slope (left) and actively controlled posture to maintain vertical (right) or to overlean and edge wheels into the slope.

4.3. Cross-slope Traverse

Characterization of Scarab as a system for difficult terrain mobility was first quantified in the laboratory in static tilt-table tests and in sandboxes (Bartlett et al., 2008). The independently actuated rocker arms of the Scarab rover allow for actively controlled roll and center-of-mass shifting relative to wheel contacts. The benefits of this feature include decreased slip during cross-slope maneuvers and increased control authority.

Table 3. Downhill Slip

Slope	Normal	Leaning	Change
10°	6%	2%	−4%
15°	22%	8%	−14%
20°	37%	15%	−22%

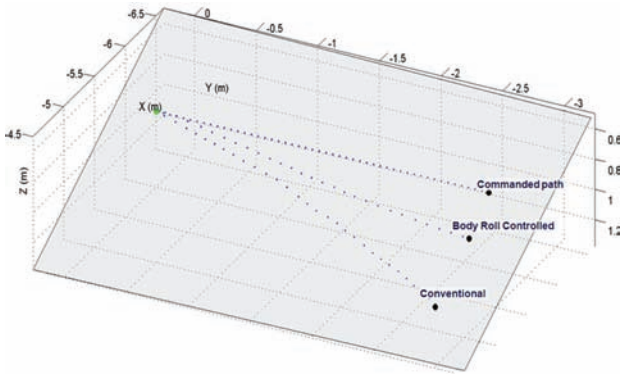

Fig. 14. Cross-slope path on at 20° incline of rover center-of-mass as commanded (constant elevation) and as measured externally when normal to the slope (conventional) and with active posture control to remain vertical with respect to gravity (body roll controlled).

Scarab was tested in cross-slope traverse normal to the slope in the conventional manner and actively controlling roll to maintain vertical posture with cross-slope of 10°, 15°and 20° (Figure 13). A surveying total station tracked a prism on the rover to millimeter accuracy and recorded instantaneous slip measurements at 1Hz. The outcome, expressed as percentage downhill slip with respect to cross-slope distance, appears in Table 3.

The considerable decrease in downhill slip (2.5 times at 20° incline as illustrated in Figure 14) arises from increased traction due to equalization of wheel loading and the reduction of the resulting shear load. The redistribution of wheel normal loads causes less sinkage and less disturbance of the soil, resulting in reduced motion resistances. We initially speculated that during "leaning" on a cross-slope, an edging effect of the wheel rim may aid traction in the transverse direction (downhill), but tests with circular profile wheels (constant ground patch shape and pressure distribution) showed that this was not the case. In addition, a result of having similar slip in all wheels in the direction of traverse is that steering mechanics are unchanged and a high degree of control authority is achieved. Conversely, when the body roll of the rover is not controlled, there are higher normal wheel loads on the downhill side of the vehicle, resulting in difficulties in controlling the vehicle to drive straight and inducing more strain on the soil. The significance of this experimental outcome lies in the ability to descend and navigate steeper slopes with while maintaining steering control. In addition, the need for explicit compensation during autonomous slope operations is obviated by the wheel slip equalization.

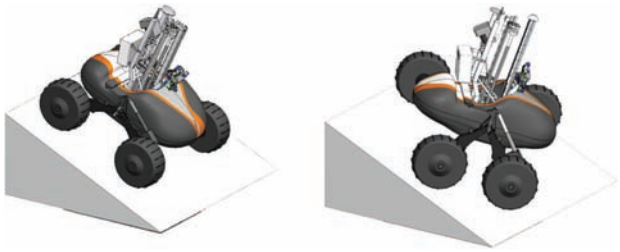

Fig. 15. Direct ascent (left, 90° angle of attack) and cross-slope ascent with actively controlled posture (right, 45° angle of attack)

4.4. Slope Ascent

In addition to improving cross-slope traverse, actively controlled center-of-mass shifting and lower angle of ascent can also increase the steepness of the slopes that are traversable. The ability to redistribute loading amongst the wheels leads to more efficient traction. Center-of-mass shifting, specifically leaning into the slope, was tested at both the Moses Lake Sand Dunes and the Mauna Kea analog sites. Inclines of loose sand, 15° or above, are normally insurmountable in direct ascent (driving straight uphill) due to weak soil strength relative to the high tractive forces demanded (Harrison et al., 2008). In order to re-distribute the vehicle weight on slopes, a method of switch-back-style maneuvering with body leaning was implemented (Figure 15). By lowering the angle of attack of the slope (driving at an angle to the maximum slope), the rover is able to use the roll degree of freedom as an advantage for slope climbing. This technique can fully equalize the wheel loading for slopes up to 35° when low angles of attack are used. In addition to wheel load redistribution, by drastically reducing the angle of attack the motion resistances and downhill component of the vehicle weight can be made perpendicular. This decreases the resulting shear load applied to the wheel and increases the slopes that can be ascended. As an example, at a non-trivial slope of 10° in low strength soil the motion resistance and gravitational resistance are approximately equal (for a medium efficiency wheel). At an extremely low angle of attack (approaching zero) this maneuver on a slope has 30% less shear stress on the wheel–soil interface. Therefore, on a 10° slope, low angle-of-attack ascent is equivalent to a 6° slope, or for the same stress, the vehicle can climb a 13° slope.

For field and laboratory experiments, evaluation of this technique was performed under the metric of heading slip: the ratio of slip in the direction the rover is commanded to travel with respect to the commanded velocity. Results from the Moses Lake and Mauna Kea field tests for direct ascent and active control of the center-of-mass shifting showed consistent decrease in the slip ratio (Table 4).

Table 4. Soil Properties Versus Slip Ratio for Direct, Active Posture, and Inch-worming Ascent. Slip for Maneuver is Slip in the Direction of Heading with Respect to Commanded Velocity. Active Center-of-Mass Control Tested with 25° (Approximate) Angle of Attack.

Performance		Slip for maneuver (%)	
Soil properties	Slope angle (degrees)	Direct ascent	Active COM control ascent
Low strength, fine volcanic ash, Mauna Kea	15	Failure, 100	Low slip, 10
	20	Failure, 100	Low slip, 30
Low strength, fine sand, Moses Lake	10	Low slip, 22	Low slip, 4
	15	Low slip 24	Low slip, 5
	20	Failure, 100	High slip, 65
Medium strength, fine sand, Moses Lake	10	Low slip, 8	Low slip, 2
	15	Low slip, 9	Low slip, 7
	20	High slip, 45	Low slip, 13

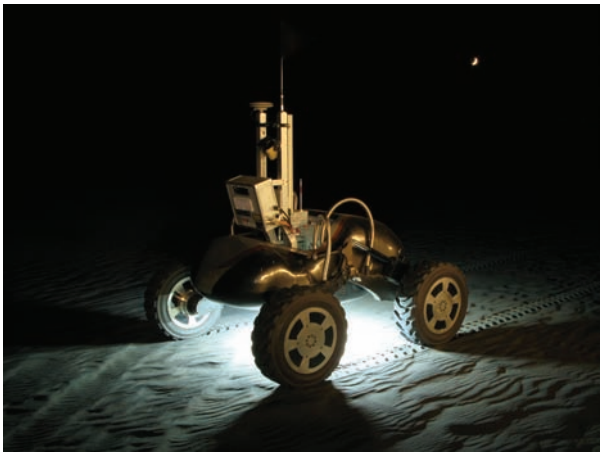

Fig. 16. Scarab navigating in darkness. The laser scanner perceives terrain ahead and an underbody optical velocity sensor estimates true velocity (without slip).

The center-of-mass shifting and low angle-of-attack heading successfully increases the steepness of slopes ascendable. The experiments were conducted with a 25° angle of attack from the horizontal. This value was determined experimentally to have adequate uphill progress and low slip on loose soil relevant to Lunar systems. It was shown that with the transformable suspension of the Scarab rover, slopes of 20° loose, dry, volcanic ash can be ascended under low slip and low risk.

5. Navigation Method and Experiments

The mission of a Lunar prospecting rover is to traverse slowly and steadily between drill sites, often without visible light or communication. Despite the short communication time delay between the Earth and Moon, about 5 seconds round trip, the rover's ability to navigate on its own is useful in many cases and necessary in a few, such as when on the floor of a polar crater. To this end we have developed terrain modeling, path planning, and motion control to enable Scarab to navigate autonomously in unknown terrain on kilometer scales.

Although the mechanism is highly capable in rough terrain, Scarab must still sense its environment so that navigation algorithms can find safe, energy efficient paths. Its vision system must provide accurate 3D information in harsh lighting conditions that occur with the low Solar incidence angle of the poles. In particular, in the polar crater environment, there will be significant areas of slope and crater floor in shadow and, in some cases, perpetual darkness. Active sensing devices are required.

In this research Scarab incorporates the TriDAR, a multipurpose 3D scanning laser system that contains both laser triangulation and laser time-of-flight modes (Taylor et al., 2009). The triangulation mode uses a continuous wave laser and known optical baseline to generate high-resolution range measurements at relatively close range. Time-of-flight measures the time required for a pulse of light to return from objects to produce medium resolution range measurements from close to far range. The TriDAR has a 30° square field-of-view and is mounted to provide imaging from the horizon to 30° below the horizon which allows imaging of the ground very near the front of the rover as well as long-range viewing (as shown in Figure 16). Range values from 1 to 30 m are collected for modeling the terrain.

Scarab scans of the terrain as determined by the navigation system after appreciable driving (more than 3 m) or turning (greater than 10°) or after time has elapsed (more than 100 s). The sensor produces a dense array of ranges and takes several seconds, so motion must stop to avoid warping the data. Laser ranging provides measurements to build models of the surrounding terrain to detect obstacles and then determine efficient and safe paths.

The Moon offers little by way of position reference. There is no network of artificial satellites, star trackers have insufficient resolution, and the terrain is barren. Scarab uses an onboard inertial measurement device (Honeywell HG1700) and optical ground speed sensor (Airrobot) (Dille et al., 2009) to enable it to estimate position and velocity with 2–3% error on distance traveled (Figure 16). In experiments in Hawaii, the optical ground speed sensor was replaced by GPS-derived velocity and produced results of similar accuracy but greater reliability.

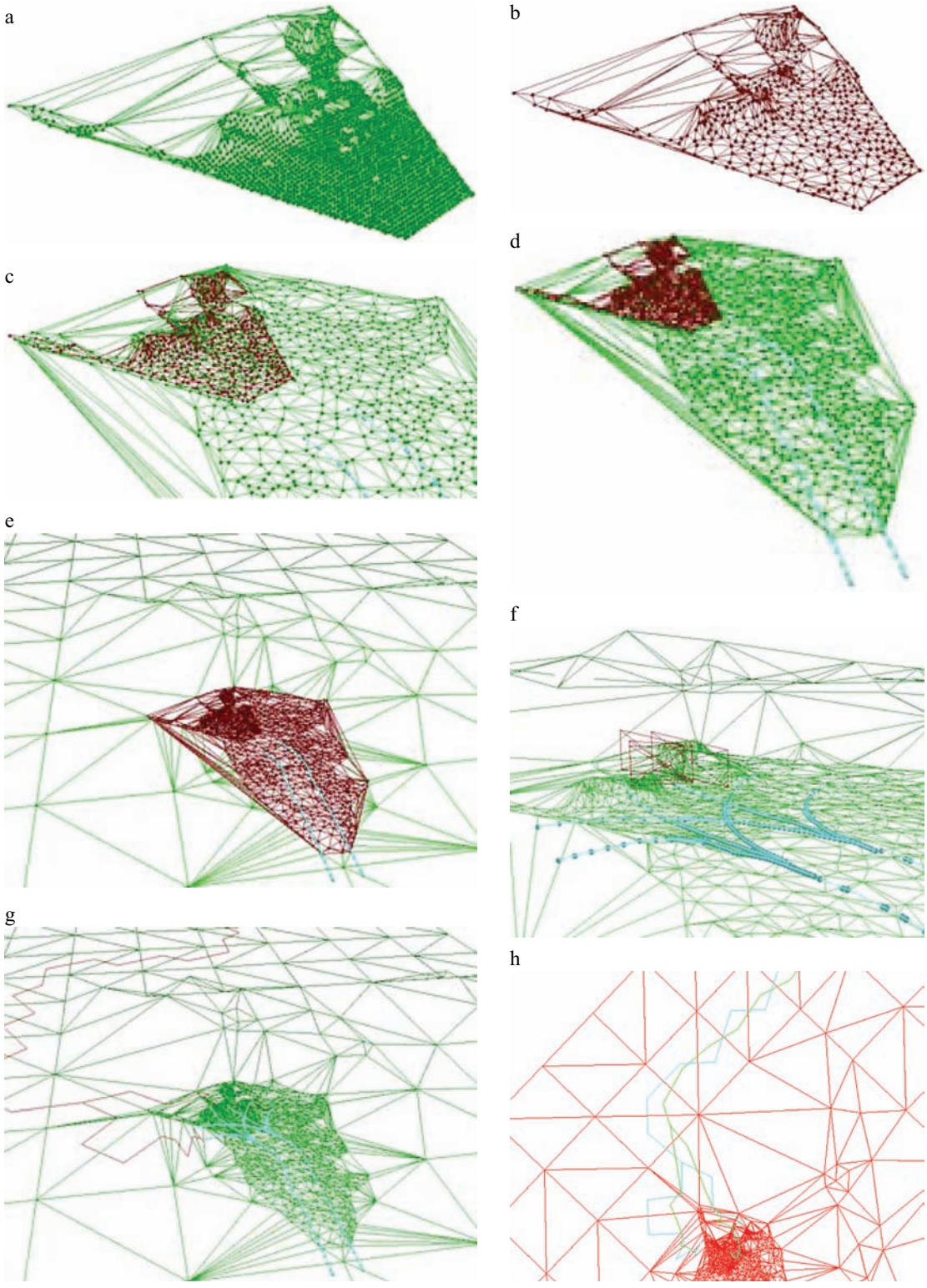

Fig. 17. a) Step 1: Filter the LIDAR scan of range measurements (point cloud) for outliers and create a dense triangulated mesh. b) Step 2: Contract the mesh, eliminating redundant values, to create a local terrain model. c) Step 3: Align the local terrain model and regional model for merging. Coarsely position the local model using pose information and associate it with the terrain profile measured by vehicle motion (cyan). Reduce the regional model to limit the overall data volume. d) Step 4: Adjust the local model (brown) to the regional model using the iterative closest point algorithm (Zhang, 1992). e) Step 5: Align the regional mesh (brown) with global mesh, which may include prior data such as an existing digital elevation models. f) Step 6: Generate forward and reverse arcs for the current rover position (cyan). Forward simulate motion along each arc to identify obstacles and evaluate traversability. g) Step 7: Search for paths from each arc in the local region to the global goal using the A* algorithm (Hart et al., 1968). h) Step 8: Improve the path using multi-step smoothing (green) such that triangle centers need not be visited (as in original cyan).

Route planning algorithms generate intermediate goals (with 30–100 m spacing) and the operator may specify multiple goals. Goals are defined as a location with radius, typically 3 or 10 m. Scarab will reach each goal region in order until it is finished or until it detects a fault condition that it cannot recover from automatically.

Autonomous navigation for Scarab is based on prior work in planetary rover navigation for continuous resource-constrained traverse (Wettergreen et al., 2005) and long-distance surveys (Wettergreen et al., 2008) both of which use stereo vision for high-density terrain observations. Laser scanning provides the same effective result: dense range measurements in a compact field of view. Our technical advance has been to develop a dynamic triangulated mesh for terrain modeling and associated algorithms for efficient triangulation, merge and reduction, in order to model 3D structure over large extent. We employ forward simulation of vehicle–terrain interaction to evaluate motion, as in Kelly and Stentz (1998). Our contribution to motion evaluation is to include posture adjustments, specifically different body heights to allow obstacle straddling and adjustments to the side frames to maintain level posture.

Triangular meshes have been applied to the modeling of natural terrain to reduce the available geometric information, for example aerial photogrammetry, to its essential form (Fayek and Wong, 1996). An advantage, as illustrated by the dense data modeled by Bakambu et al. (2006), of triangular meshes is that resolution can vary with the amount of information, specifically the complexity of terrain.

One of the challenges in this work is that the rover must continuously generate new meshes as it encounters new terrain. This requires a cycle of mesh generation and then merging with prior meshes. In our work we use the rover position estimate for initial alignment and then the iterative closest point algorithm (Zhang, 1992) for fine correction of position and orientation. We should note that we are not currently performing simultaneous localization with the mapping operation, largely because position in the fixed world frame is not precisely required.

For planning paths, Pimenta et al. (2007) use a triangulated planar map of traversal cost to achieve variable resolution, primarily for path planning efficiency (Periera, 2009). The work here considers 3D meshes. Dupuis et al. (2008) use A* search on a triangular mesh to determine a path to the goal although without smoothing the path, although this usually means that many point turns are required. Scarab is controlled like other continuous-motion, continuous-steering rovers we have developed (Wettergreen et al., 2008) and also performs arc selection in the near field and then graph search over long range to the goal. Its arcs and paths are smoothed for power and time efficiency.

The rover navigation system iterates steps that build a mesh of new observations of local terrain, merge this with recent observations of the surrounding terrain, and evaluate traversability. Search to the global goal along with forward simulation of potential driving arcs selects the arc that makes best progress to the goal.

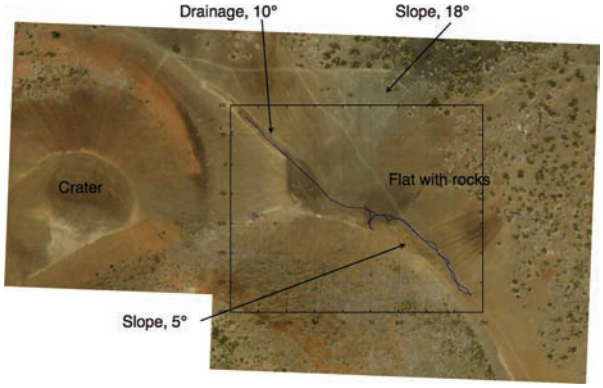

Fig. 18. Autonomo0us traverse on Mauna Kea covering 978 m including descent of a 10° drainage and negotiation through obstacle field and varying slopes +/-5°.

This navigation method is described and illustrated in Figure 17 (a to h), in which each step is a transformation of data that produces rover driving commands from initial terrain range measurements. This process iterates approximately every 10 seconds as the rover drives. It is implemented on a single Pentium3, 800 MHz processor with 256 MB of RAM, utilizing about 50% of available CPU cycles.

Each scan of range points from the LIDAR is used to build a local terrain model. The points are filtered (to remove noise and outliers), transformed into the rover's coordinate frame, and triangulated into a mesh (Chew, 1987). The mesh is then reduced by eliminating redundant points, those points that add no significant information. Finally the mesh is aligned with prior data using iterative closest point to generate the terrain model that is used to identify obstacles and select the best path to the goal. Many candidate vehicle motions are evaluated in the near- and far-field. The near-field analysis involves forward simulating vehicle motion on the mesh to identify collision and slope hazards and assess their severity. The far-field analysis applies A* search to estimate the progress of each potential move towards the goal. The search cost function combines safety in the near-field with progress in the far-field. A guiding principle in this work is that space-relevant software must be computationally and conceptually simple in order to apply under severe resource and risk constraints. Rover navigation algorithms operate in real-time.

Our experimental approach has been to conduct 1 km traverses in a variety of terrains. At both the Moses Lake and Mauna Kea sites, Scarab autonomously completed the following objective: travel at least 3 km at night and descend into an analog crater. Traverses are kilometer scale and performed after sunset, they account for most of the total distance traveled at each site although many short experiments were also conducted. Crater descent was conducted with a long (100 m) traverse that included descending a steep (10°) slope.

Fig. 19. Images of the terrain model with actual rover tracks, in cyan, overlaid (left) and photographs of Scarab while autonomously descending into a 9-m deep by approximately 100-m diameter sand pit (right). Terrain model constructed with triangular mesh in real-time for rover navigation and then re-rendered with atmosphere and light for an illustrative comparison.

Scarab completed a total of 3.6 km in 27 traverses in Washington State. The first dark traverse was 1.2 km with four interventions due to sensor faults and one due to a controller error. These faults were recoverable; they did not jeopardize the rover and are easily resolved by resetting a device, something that could be accomplished remotely. A second dark traverse used an alternative navigation algorithm (Pedersen et al., 2008) and completed 1.1 km with two interventions due to localization errors.

Scarab traveled 3.0 km in 20 traverses on Mauna Kea, most of this was accomplished during two overnight traverses. The first dark traverse was split into two parts: 199 m of crater descent followed, after a pause, by 779 m of traverse before stopping at the drill site but with a software fault. A second overnight traverse was also interrupted; the first part being 312 m and stopped on a software fault, the second was 989 m and ended with a CANBus fault. Although it may seem problematic for faults to occur, each of these night traverses exceeded 8 hours of continuous operation in complex natural terrain and unexpected events do occur. It is significant that all faults were non-fatal and could be rectified remotely.

At each site, Scarab autonomously completed a simulated crater descent using the available analog terrain. At Moses Lake, Scarab drove into a 9-m deep pit with 10–20°sloped sides. (Figure 19) This was safely accomplished including two autonomous switchback maneuvers. At Mauna Kea, Scarab repeatedly drove down a winding drainage channel. The route was over 100 m long and descended over 25 m with a uniform grade of 10–15°.

Traverse termination conditions for both field tests are shown in Figure 20. No interventions were required to stop the vehicle from driving into a hazard (zero emergency stops). At Moses Lake, most traverses (15 of 25) ended with a recoverable fault, primarily from periodic communication failures with the terrain sensor. On Mauna Kea reliability was improved by automatically recovering from communication faults. Most traverses ended by reaching

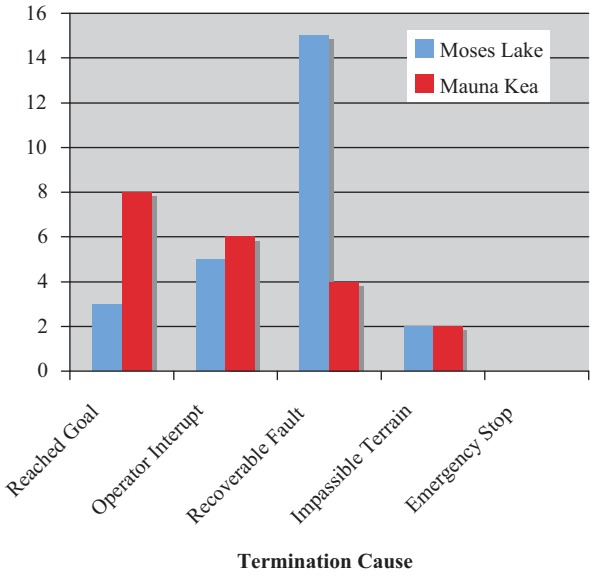

Figure 20. Termination conditions in autonomous navigation experiments.

the goal (8 of 20) or stopping the traverse for other reasons (6 of 20) associated with test logistics or operator assessment of system performance. Recoverable faults are those that can be remotely corrected and thus would not be mission ending in a Lunar scenario. Similarly most operator interrupts would not occur in a Lunar context.

These field results are far from perfect but indicate that reliability is improving and will reach the level of previous planetary rover prototypes despite the high degree of autonomous capability.

6. Conclusion

The Scarab rover has been uniquely configured for the transport and stabilization of a coring drill and associated soil analysis instruments for Lunar crater exploration. By building Scarab and conducting hundreds of hours of field experiments in Washington State and Hawaii we have learned and demonstrated principles and new capabilities.

Experiments have quantified the rover's drawbar pull and slope climbing ability as well as power required for these activities under a variety of Lunar-like soil and terrain conditions. The benefits of central-mounting and active body height and roll control are apparent in deployment of the drill. Mechanical release provided by the differencing linkage maintains all wheels on the ground while still allowing skid steering in rough natural terrain.

The efficacy of passive pitch averaging with skid steering and the benefits of active roll control for slope ascent and descent are established. Experiments involving different traction surfaces, wheel diameters, and ground pressures have shown a large range of drawbar pull values. Differences of 50% have been achievable through traction surface/grouser modifications. Lowering ground pressure and reducing sinkage has increasing effects on traction but results in large differences in driving power (up to 50% during experiments). Drawbar pull tests performed as lab and field experiments have highlighted the wheel design as a leading element in tractive and power design requirements.

Active control of posture and leaning into the slope while taking a moderate angle of attack are shown to increase the steepness of ascendable slopes by as much 20%. Inch-worming is also shown to have specific applicability and to dramatically increase drawbar pull, in some instances doubling the maximum load. Inch-worming also suggests novel methods of escaping entrapment once wheels are buried and spinning.

Field demonstrations have also proven the capability of the laser-based perception and navigation system for kilometer-scale autonomous traverse, including autonomous descent into craters. New capabilities for performing switchback maneuvers and for straddling some obstacles have also been shown. Long traverses most frequently end in successfully reaching the goal location but in those cases where a fault occurs it has been recoverable through a remote command, as would be possible on the moon. In total the mobility and navigation requirements for a Lunar-surface prospecting mission have been demonstrated in analog terrain.

Acknowledgments

We gratefully acknowledge the contributions of our technical team and the assistance of Paul Bartlett, Antonio Delfino, Bill Bluethmann, Dale Boucher, John Caruso, Colin Creager, Adam Deslauriers, Ross Hudson, Jaret Matthews, Jean-Paul Meraldi, Jacqueline Quinn, David Roberts, Gerald Sanders, Spencer Spiker, Ross Taylor, Bart Thompson, Chuck Whittaker, and William Whittaker. This research was supported by NASA under grants NNX07AE30G to Vivake Asnani, Program Scientist, and NNX08AJ99G to Robert Ambrose, Program Scientist.

References

Bakambu, J.N., Allard, P. and Dupuis, E. (2006) 3D terrain modeling for rover localization and navigation. *The 3rd Canadian Conference on Computer and Robot Vision*, 2006.

Bartlett, P., Wettergreen, D. and Whittaker, W. (2008) Design of the Scarab rover for mobility and drilling in Lunar cold traps. *International Symposium on Artificial Intelligence, Robotics and Automation in Space (i-SAIRAS)*, Los Angeles, CA, February 2008.

Bartlett, P. (2008) *Kinematic Suspension Design for Planetary Surface Vehicles*. Technical Report CMU-RI-TR-08-20, Carnegie Mellon University, Robotics Institute, May 2008.

Bekker, M. (1956) *Theory of Land Locomotion*. Ann Arbor, MI, The University of Michigan Press.

Boucher (2008) Space Exploration - Drilling Technology, http://www.norcat.org/Innovation-space.aspx, November 2008.

Chew (1987) Constrained Delaunay Triangulation, Algorithmica, Volume 4, Numbers 1-4, New York: Springer, June 1989.

Clark, R. (2009) Detection of adsorbed water and hydroxyl on the Moon. *Science*.

Dille, M., Grocholsky, B. and Singh, S. (2009) Outdoor downward-facing optical flow odometry with commodity sensors. *Field and Service Robotics*, Boston, MA, July 2009.

Dupuis, E., Rekleitis, I., et al. (2008) Over-the-horizon autonomous rover navigation: experimental results. *International Symposium on Artificial Intelligence, Robotics and Automation in Space (i-SAIRAS)*, Los Angeles, CA, February 2008.

Fayek, R. and Wong, A. (1996) Using hypergraph knowledge representation for natural terrain robot navigation and path planning. *International Conference on Robotics and Automation*, Minneapolis, MN, April 1996.

Fong, T. et al. (2008) Field testing of utility robots for lunar surface operations. *AIAA Space*, 2008.

Fox, R., Schowengerdt, F. and Hamilton, J. (2009) A high-quality Lunar analog experience. *Planetary and Terrestrial Mining Sciences Symposium*, 2009

Furlong, P., Howard, T. and Wettergreen, D. (2009) Model-predictive control for mobile robots with actively reconfigurable chassis. *Field and Service Robotics*, Boston, MA, July 2009.

Harrison, D., Ambrose, R., Bluethmann, B., and Junkin, L. (2008) Next generation rover for Lunar exploration. *IEEE Aerospace Conference*, Big Sky, MT, 2008.

Hart, P., Nilsson, N. and Raphael, B. (1968) A formal basis for the heuristic determination of minimum cost paths. *IEEE Transactions on Systems, Science and Cybernetics*, **4**(2): 100-107.

Iagnemma, K. and Dubowsky, S. (2004) *Mobile Robots in Rough Terrain: Estimation, Motion Planning and Control with Application to Planetary Rovers*. Berlin, Springer-Verlag, 2004.

Iagnemma, K., Rzepniewski, A., Dubowsky, S., Pirjanian, P., Huntsberger, T. and Schenker, P. (2000) Mobile robot kinematic reconfigurability for rough-terrain. *Proceedings of SPIE*.

Kelly, A., and Stentz, A. (1998) An approach to rough terrain autonomous mobility. *Autonomous Robots*.

Lindemann, R. and Voorhees, C. (2005) Mars Exploration Rover mobility assembly design, test and performance. *International Conference on Systems, Man, and Cybernetics*, Hawaii, October 2005.

Muscatello, A. et al. (2009) Lunar water resource demonstration. *47th AIAA Aerospace Sciences Meeting*, Orlando, FL, January 2009.

Nabbe, B. and Hebert, M. (2007) Extending the path-planning horizon. *The International Journal of Robotics Research*, **26**(10): 997-1024.

Oravec, H. A., Asnani, V. and Zeng, X. (2009) Design and characterization of GRC-1: A soil for lunar terramechanics testing in Earth-ambient conditions. *Journal of Terramechanics*, submitted.

Pedersen, L. et al. (2008) Dark navigation: sensing and rover navigation in permanently shadowed Lunar craters. *International Symposium on Artificial Intelligence, Robotics and Automation in Space (i-SAIRAS)*, Los Angeles, CA, February 2008.

Periera (2009)

Pieters, C. et al. (2009) Character and spatial distribution of OH/H_2O on the surface of the Moon seen by M^3 on Chandrayaan-1. *Science*.

Pimenta, L., Pereira, G. and Mesquita, R. (2007) Fully continuous vector fields for mobile robot navigation on sequences of discrete triangular regions. *IEEE International Conference on Robotics and Automation*, Rome, April 2007.

Rekleitis, I., Bedwani, J.-L. and Dupuis, E. (2009) Autonomous planetary exploration using LIDAR data. *IEEE International Conference on Robotics and Automation*, Kobe, Japan, May 2009.

Rollins, E., Luntz, J., Foessel, A., Shamah, B. and Whittaker, W. (1998) Nomad: a demonstration of the transforming chassis. *IFAC Workshop on Intelligent Components for Vehicles*, Seville, Spain, March 1998.

Sanders, G. et al. (2009) In Situ Resource Utilization (ISRU) Program. *47th AIAA Aerospace Sciences Meeting*, Orlando, FL, January 2009.

Spudis, P. (2006) Ice on the Moon. *Space Review*.

Taylor, R., et al. Multipurpose 3D sensor for planetary rover missions. *International Aerospace Congress*, Korea, October 2009.

Tarokh, M. and McDermott, G. (2007) A systematic approach to kinematics modeling of high mobility wheeled rovers. *IEEE International Conference on Robotics and Automation Rome*, April 2007.

Von Sybel, H., and Gross-Scharmann, F. (1961) Triebkraftsteigerung bei Gelanderfahrzeugen durch das Schub-Schritt-Verfahren (Increased draft for wheeled vehicles operating outside the roadway by the 'thrust-stride-system'). *International Conference on Terrain–Vehicle Systems*, Torino, 1961.

Wettergreen, D., et al. (2005) Sun synchronous robotic exploration: technical description and field experimentation. *The International. Journal of Robotics Research*, **24**(1): 3–30.

Wettergreen, D., et al. (2008) Long-distance autonomous survey and mapping in robotic investigation of life in the Atacama. *International Symposium on Artificial Intelligence, Robotics and Automation in Space (i-SAIRAS)*, Los Angeles, CA, February 2008.

Wettergreen, D., et al. (2009) Field experiments in mobility and navigation with a Lunar rover prototype. *Field and Service Robotics*, Boston, MA, July 2009.

Wilcox, B. and Jones, R. (2000) The MUSES-CN Nanorover Mission and related technology. *IEEE Aerospace Conference*, Big Sky, MT, 2000.

Wilcox, B., Litwin, T. Biesiadecki, J., Matthews, J., et al. (2007) Athlete: a cargo handling and manipulation robot for the Moon. *Journal of Field Robotics*.

Wong, J. (2001) *Theory of Ground Vehicles*. New York, Wiley Interscience.

Zhang, Z. (1992) Iterative point matching for registration of free-form curves. *IRA Research Reports*, No. 1658, Program 4: Robotics, Image and Vision.